JOURNAL OF MATERIALS SCIENCE 18 (1983) 483–492

Structural characterization of rapidly solidified white cast iron powders

LAWRENCE E. EISELSTEIN,* OSCAR A. RUANO,† OLEG D. SHERBY
Department of Materials Science and Engineering, Stanford University, Stanford, California 94305, USA

Three white cast iron alloy powders (2.4% C, 3.0% C, and 3.0% C + 1.5% Cr) manufactured by a rapid solidification processing technique were investigated. It was found that the microstructures of all three alloy powders were similar. The primary constituent of these powders was found to be retained austenite. Only small amounts of carbide and martensite were found in the rapidly solidified white cast iron powders. The primary austenite cells and dendrites that nucleate and grow from the melt are retained upon cooling to room temperature with little carbide precipitation. The low volume fraction of marensite found was due to the high carbon concentration of the austenite. A fine dispersion of carbides in an austenite matrix is formed as a result of the solidification of the eutectic liquid in the intercellular and interdendritic regions. The relative proportion of primary austenite to eutectic can be explained by the carbon segregation that occurs during the solidification of the primary austenite. Annealing of the powders at 650° C transforms the metastable austenite into alpha iron and carbide. The carbides have a bimodal distribution with small carbides precipitating within the primary austenite cells and dendrites and large carbides precipitating within the intercellular and interdendritic regions.

1. Introduction

Rapid solidification technology (RST) offers a unique method of controlling the structure and properties of materials. Amorphous phases, metastable phases, increased solid solubility of alloying elements, and unusually fine structures can be obtained by this type of processing. Many methods of producing RST metals and alloys have been developed [1–3]. These include splat quenching, spin melting, roll quenching, electron or laser glazing, and centrifugal atomization.

Work on warm compaction of white cast irons produced from rapidly solidified powders has shown that the carbides in these materials can be maintained at sizes less than 5 μm [4, 5]. Attainment of fine structures in such white cast irons can lead to superplastic behaviour [4, 5].

The present investigation is concerned with the characterization of the microstructure, annealing behaviour and constituent phases of three white cast irons produced by one such RST process.

2. Materials and experimental techniques

By definition, white cast irons must contain at least 2.1% C, which is the maximum equilibrium solid solubility of carbon in austenite [6]. The carbon must be also present in the form of carbides rather than in the form of graphite. The three white cast iron powders chosen contained 2.4% C, 3.0% C, and 3.0% C + 1.5% Cr. The chemical compositions of these powders are listed in Table I. The silicon and nickel contents of the cast irons investigated were kept low since these elements promote graphitization [7]. Chromium was added to one of the cast irons because it is a carbide stabilizer, inhibits carbide growth, and therefore this chromium-containing cast iron may be expected to have a very fine carbide microstructure.

*Present address: SRI International Menlo Park, California 94025, USA.
†Present address: Centro Nacional de Investigaciones Metalurgicas, Av. de Gregorio del Amo s/n, Madrid-3, Spain.

0022–2461/83/020483–10$03.70/0

TABLE I Chemical composition of white cast irons investigated

Alloy	C	Cr	Si	Mn	P	S
2.4% C	2.36	0.018	0.14	0.92	0.014	0.014
3.0% C	3.04	< 0.005	0.08	0.51	0.006	0.004
3.0% C + 1.5% Cr	3.03	1.49	0.09	0.61	0.005	0.009

The white cast iron powders were obtained by the rapid solidification process developed by Pratt and Whitney Aircraft (known as "Rapid Solidification Rate" or RSR). This process involves forced convective cooling of the powders which produces quenching rates that vary with particle size and alloy composition. Typically, the quenching rates are greater than 10^5° C sec^{-1} if the powder particles are smaller than 100 μm diameter [8].

The RST powders were first sieved to remove powder particles greater than 100 μm. By using standard ASTM methods [9], it was determined that the average powder particle size was 55 μm for all three sieved batches of RST white cast irons. Small quantities of some of these powders were cooled to liquid nitrogen temperature (− 196° C). Other small amounts were vacuum heat-treated at 650° C at various times in order to investigate the effect of thermal treatments on the structure of the RST white cast irons. The thermally treated powders were cold-mounted in epoxy for microstructural studies by optical and scanning electron microscopy (SEM). During the curing stage, the epoxy temperature was monitored and kept below 75° C to minimize the tempering of the powder. The samples were then polished and etched in 5% nital. For SEM examination, gold was evaporated on to the polished and etched surface. Microhardness measurements were made with a Vickers diamond pyramid indentor at a load of 200 g. A minimum of five microhardness measurements were taken on each sample to obtain an average hardness. X-ray diffraction (XRD) was done on 2.4% C and 3.0% C + 1.5% Cr RST white cast iron powders less than 45 μm diameter. Lattice parameter determinations were obtained at room temperature using appropriate extrapolation functions [10].

3. Results

The morphology, microstructure, and constituent phases present in the RST white cast irons are described in this section along with the results on the microhardness as affected by quenching in liquid nitrogen and tempering at 650° C.

3.1. Morphology

Typical morphologies obtained in the powders are shown in Fig. 1. The majority of powder particles are spheroidal (Fig. 1a). Some particles show porosity as illustrated in Fig. 1b. A small fraction of the particles have irregular shapes consisting of two types of morphology. The first type (Fig. 1c) is a deformed spheroidal shape showing indications of collisions with other particles while still hot. The second type (Fig. 1d) is a fragmented spheroidal shape suggesting that particle collisions took place at a low temperature where fracture could occur.

3.2. Microstructure

Three distinct types of microstructures were observed in the as-received RST white cast irons. Typical microstructures of the 2.4% C and 3.0% C RST white cast iron are shown in Figs. 2 and 3, respectively. The microstructures present in the 3.0% C + 1.5% Cr RST powder were similar to the 3.0% C RST powders and therefore will not be discussed.

Three categories of microstructure were observed in the 2.4% C powders and can be discussed as follows: (1) a cellular microstructure which is shown in Fig. 2a and b, (2) a dendritic microstructure which is shown in Fig. 2c and d, and (3) an acicular, needle-like microstructure which is shown in Fig. 2e. Typically, each powder particle could be classified into one of these microstructural categories. Some individual particles, however, exhibited a microstructural mixture consisting of cells and dendrites. Acicular microstructures were only found in the small powders (< 20 μm). Other than the appearance of the acicular microstructure in the small particles, there was no noticeable difference in the ratio of cellular to dendritic microstructures for different particle sizes.

The 3.0% C powders revealed similar microstructures to the 2.4% C powders except that the acicular microstructure was never observed.

The cell size and secondary dendrite arm spacing (see Fig. 2b and d) are noted to decrease as

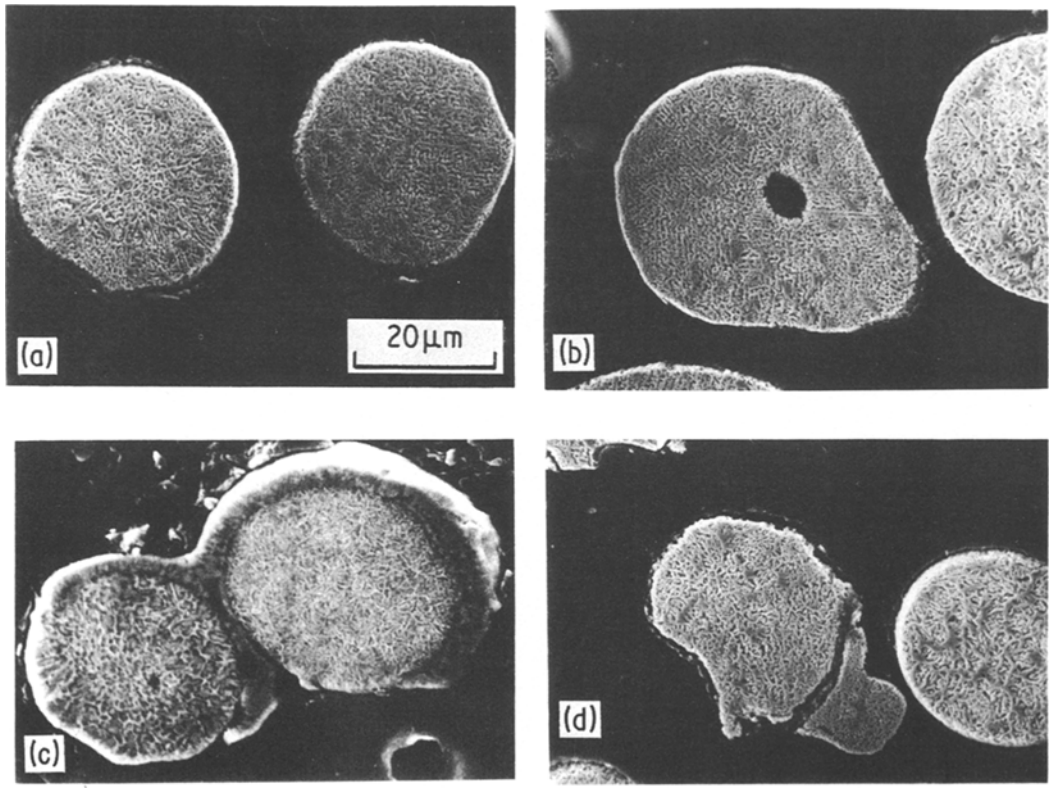

Figure 1 Powder particle morphologies of RST white cast irons.

the particle size is decreased for all three RST white cast irons. The interdendritic and intercellular regions (Fig. 2b and d) are, in general, featureless. Some of the powder particles with thick ($> 2\,\mu m$) interdendritic or intercellular regions show the presence of two phases in the form of striations as observed in Fig. 3a and b.

The microstructure of the powders as originally received did not change significantly upon liquid nitrogen cooling. The microstructure remained essentially the same, except that the volume fraction of martensite increased slightly over that observed for the powders in the as-received condition. Fig. 3a shows an example of martensite plates formed in a large cellular type of microstructure. In powder particles with fine microstructures, i.e., mean free paths $< 5\,\mu m$, no obvious indications of martensite were observed.

A large microstructural change was observed to occur when the powder particles were annealed at 650° C for 15 min. Fig. 4 shows the annealed microstructure that is developed in the 2.4% C and 3.0% C white cast irons after 15 min at 650° C. The microstructural features in the annealed powder are much finer than those observed in powders in the as-received condition. The phases present are now ferrite and carbide. The light appearing regions are carbides.

3.3. Microhardness

Fig. 5 shows the hardness of the as-received and liquid nitrogen cooled white cast iron powders, as well as the change in microhardness on annealing at 650° C. The Vickers microhardness of the RST white cast irons in the originally received condition was about $630\,kg\,mm^{-2}$ for the 2.4% C material and $1000\,kg\,mm^{-2}$ for the 3.0% C + 1.5% Cr material. The liquid nitrogen cooled materials have greater hardnesses than those of the white cast irons in the as-received condition ($750\,kg\,mm^{-2}$ and $1100\,kg\,mm^{-2}$ for the 2.4% C and 3.0% C + 1.5% Cr materials, respectively). These microhardness values are considerably higher than the value of $400\,kg\,mm^{-2}$ reported for typical white cast irons with even higher alloy content [11, 12].

Annealing the white cast iron powders at 650° C results in an initial rapid microhardness decrease. After 15 min, however, the softening rate decreased considerably. After annealing at

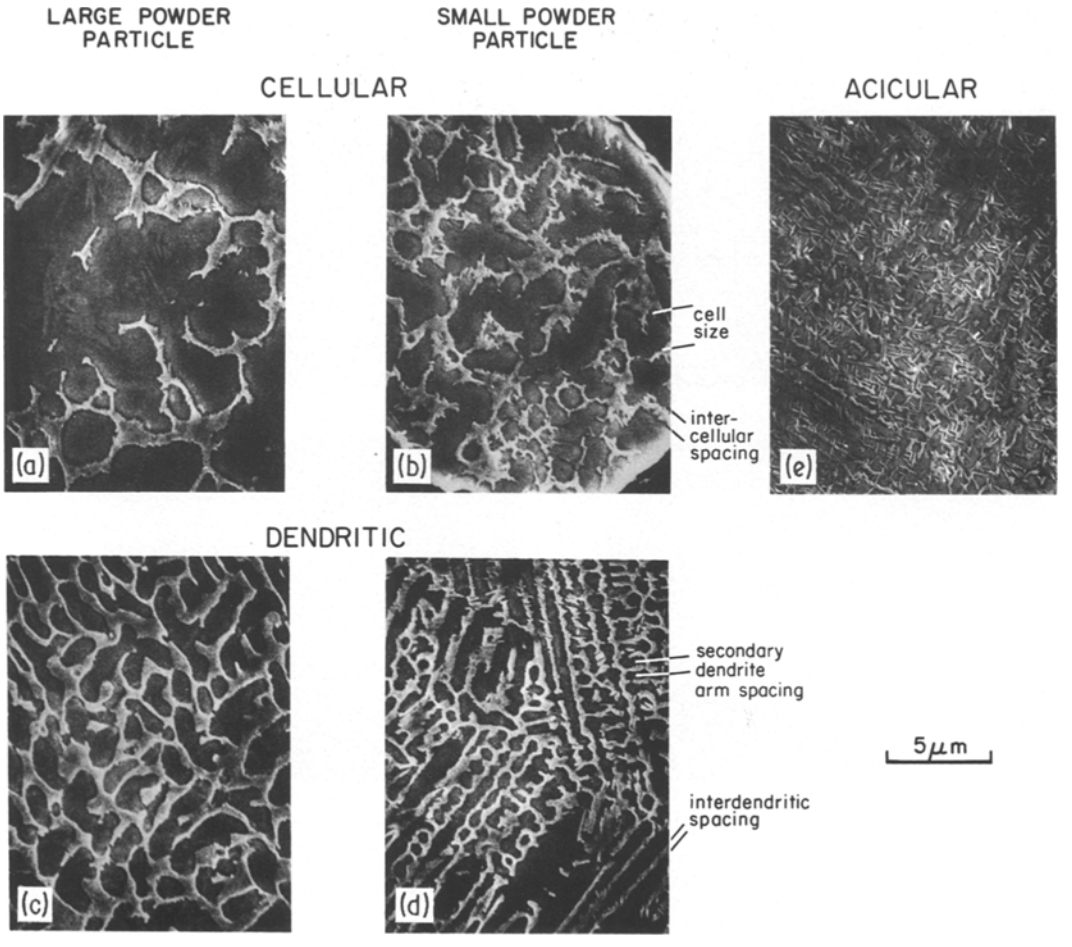

Figure 2 Microstructure of large and small 2.4% CRST white cast iron powder particles. (All microstructures at the same magnification.)

650° C for 4 h the microhardness is 400 and 510 kg mm^{-2}, respectively, for the 2.4% C and 3.0% C + 1.5% C RST white cast irons.

3.4. X-ray diffraction

X-ray diffraction examinations were conducted on the 2.4% C and 3.0% C + 1.5% Cr RST white cast irons in the following three conditions: as-received, liquid nitrogen cooled, and annealed (650° C/30 min). The examinations indicated that powders in the as-received condition and in the liquid nitrogen cooled condition contained mainly retained austenite. Weak carbide diffraction peaks were observed which is attributed to the fineness of the carbides present in the powders. Although martensite plates were observed in the as-received and liquid nitrogen cooled 2.4% C and 3.0% C + 1.5% Cr RST alloys, martensite peaks could not be detected by X-ray diffraction. This was due to the relatively low volume fraction of martensite present in these powders.

The lattice parameter of the retained austenite was measured to be 0.3633 ± 0.0003 nm and 0.3626 ± 0.0003 nm for the 2.4% C and the 3.0% C + 1.5% Cr white cast irons, respectively.

The dependence of the lattice parameters of austenite on carbon, nickel, and chromium is given by the following equation [13]:

$$a_0\,(\text{Å}) = 3.5780 - 0.002\,(\%\text{Ni}) + 0.006\,(\%\text{Cr}) + 0.033\,(\%\text{C}).$$

This equation makes it possible to calculate the amount of carbon dissolved in the retained austenite. In turn, these calculations show that the carbon content of the retained austenite is 1.67 ± 0.10% C and 1.43 ± 10% C for the 2.4% C and 3.0% C + 1.5% Cr RST white cast irons, respec-

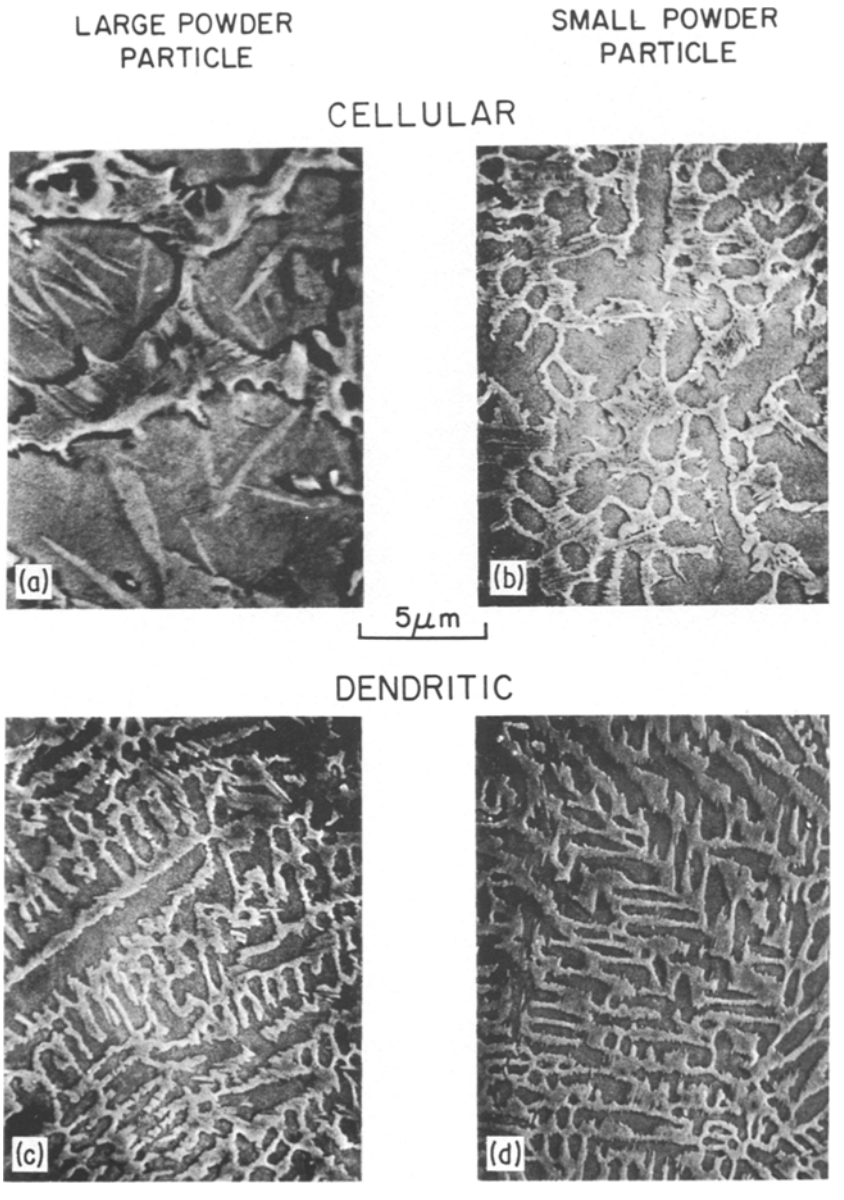

Figure 3 Microstructure of large and small 3.0% C RST white cast iron powder particles.

tively. These values are less than the maximum equilbrium solubility of carbon in austenite for both alloys (2.1% C for the 2.4% C and 1.5% C for the 3.0% C + 1.5% Cr). This indicates that carbides must be present in the intercellular or interdendritic regions of the RST powder particles in the as-received conditions.

The annealed powders were found to have only sharp ferrite and carbide X-ray diffraction peaks present.

4. Discussion

At equilibrium, or near-equilibrium, the iron–carbon phase diagram indicates that the RST white cast iron powders should contain ferrite and graphite or metastable carbide at room temperature. All three alloys at room temperature should contain more than 35 wt % carbide. Under rapid solidification conditions, metastable phases other than carbide can be retained at room temperature. It has been shown that martensite, austenite, delta iron, epsilon iron and even amorphous iron–carbon can be obtained in eutectic or near eutectic composition rapidly solidified iron–carbon alloys at room temperature [14–16]. Other effects such as solute segregation

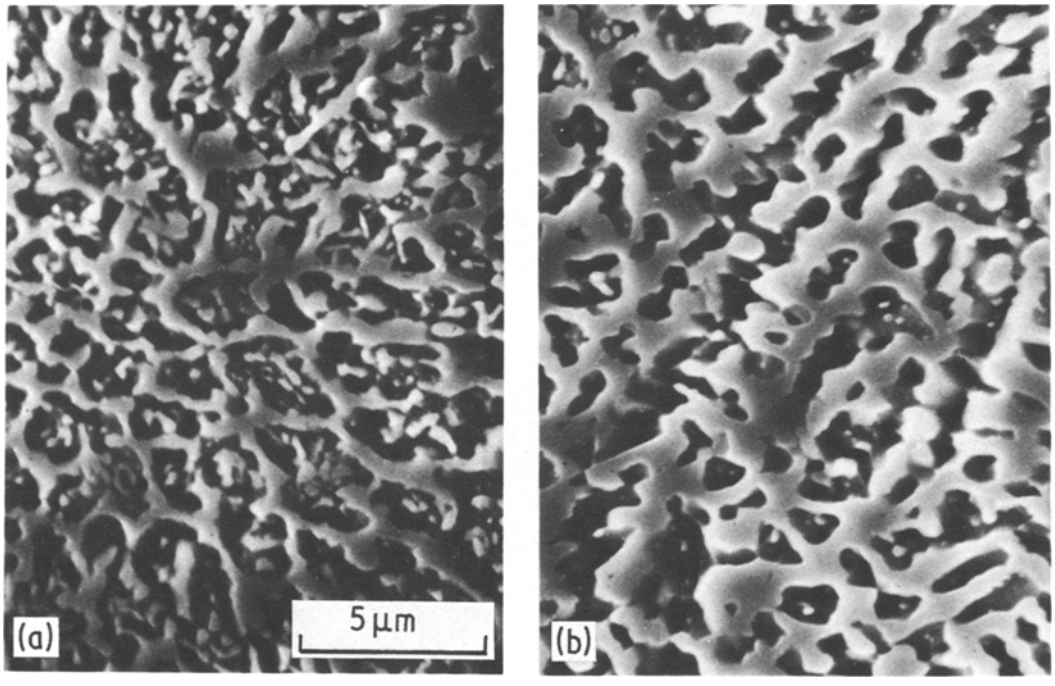

Figure 4 Microstructure of 2.4% C and 3.0% C RST white cast iron powder particle after annealing at 650° C for 15 min. (a) 2.4% C powder, and (b) 3.0% C powder. (Both microstructures at the same magnification.)

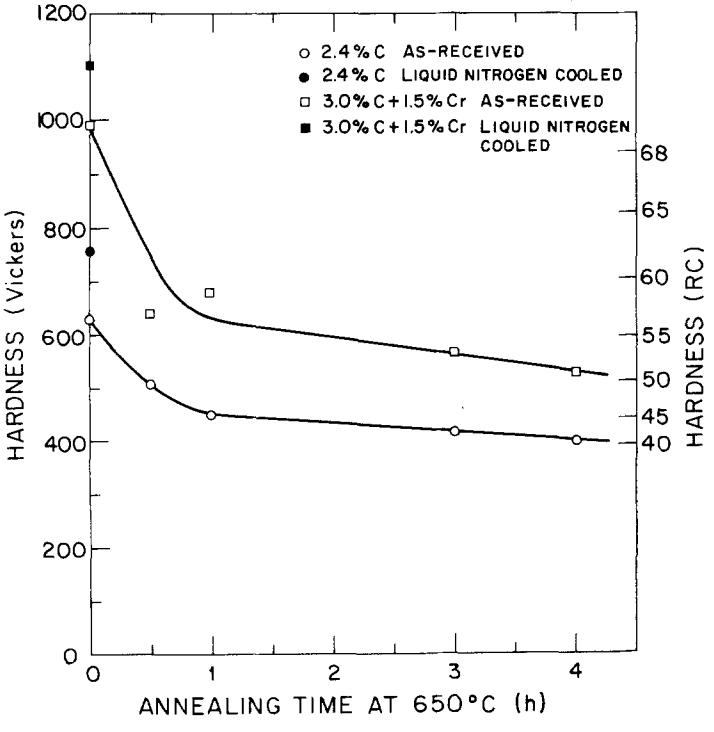

Figure 5 Microhardness at room temperature of RST white cast irons as a function of annealing time at 650° C.

[17, 18] and the formation of "micro-crystalline regions" [18, 19] could have a significant influence on the microstructure of rapidly solidified metals. The following discussion attempts to explain what effect rapid solidification had on the retention and morphology of the metastable phases. In addition, the volume fraction of phases present is considered in the light of solute segregation. The effect of annealing on the microstructure of the powder particles is also discussed.

4.1. Retention and morphology of metastable phases

Retained austenite in the form of cells or dendrites is a major constituent of all three RST white cast irons investigated, as determined from X-ray diffraction measurements. The retained austenite is seen as the dark regions in the SEM photomicrographs (Figs. 2 and 3). The presence of lenticular martensite in the dark regions (e.g. Fig. 3a) verifies that such regions are retained austenite. The bright regions are ledeburite (a eutectic mixture of retained austenite and carbide) and will be discussed later.

Cellular or dendritic solidification structures are believed to be determined by the thermal gradient, G, at the solid–liquid interface and the solidification velocity, R [3, 17]. At relatively high thermal gradients or at relatively low growth velocities, cellular structures are preferred over dendritic structures. If, however, the solidification rate ($G \cdot R$) is so fast that the critical undercooling required for homogeneous (diffusionless) solidification is reached, then structures termed "microcrystalline" appear [18, 19]. These "microcrystalline" regions have been reported to occur in some rapidly solidified alloys [18].

The combination of temperature gradient and solidification rates experienced by the RST powders in this investigation was such that only cells or dendrites were observed (Figs. 2 and 3). It appears, therefore, that the solidification rate was not rapid enough for "microcrystalline" or amorphous solidification to occur in these alloys.

The cell size and secondary dendrite arm spacing is know to depend on cooling rates. Figs. 2 and 3 clearly illustrate that as the cooling rate increases (i.e., as the particle size decreases), the cell size and secondary dendrite arm spacing decrease. Using the data of Suzuki [20] and choosing 1 μm as being representative of the spacing between secondary dendrite arms, a cooling rate of $3.3 \times 10^5\,^{\circ}\mathrm{C\,sec^{-1}}$ is obtained. This cooling rate is quite close to the rates reported for other RSR processed alloys [8].

Martensite plates were generally observed in the largest of the austenite cells and dendrites, as, for example, shown in Fig. 3a. The martensite start temperature for these alloys can be calculated from a knowledge of the austenite chemistry. If all alloying elements are uniformly distributed, the martensite start temperature [M_s] can be estimated [21–23]. In order to calculate the M_s temperature, the carbon content in the austenite was determined by X-ray diffraction measurements for the 2.4% C and 3.0% C + 1.5% Cr alloys. The following values were obtained: 1.67% C for the 2.4% C powder and 1.43% C for the 3.0% C + 1.5% Cr powder. Although the carbon content of retained austenite in the 3.0% C powder was not determined, it was assumed to be equal to the value measured for the 2.4% C powder. Using these values, the M_s temperature was calculated as -196, -183 and -102° C for the 2.4% C, 3.0% C and 3.0% C + 1.5% Cr, respectively. The calculated M_s temperatures are substantially below room temperature and, therefore, no martensite should be found in the as-received powders at room temperature. Since some martensite was found, it is believed that some plastic deformation occurred in these particles which helps to nucleate the martensite above its M_s temperature. The plastic deformation is probably the result of the thermal strains experienced by the powder during rapid solidification and cooling. Alternatively, the deformation could also be the result of the mechanical strains arising from particle collisions (Fig. 1b and c) during RST processing.

Cooling the as-received powder particles to -196° C results in a small increase in the martensite volume fraction. This was deduced from the increase in microhardness (Fig. 5). This small increase in microhardness is in agreement with SEM observations of large particles where approximately 10% of martensite is present in the retained austenite. Virtually no martensite was observed in the small particles. The likely reason for the small amount of martensite present in the liquid nitrogen cooled powders is due to the stabilization of austenite caused by ageing at room temperature for several months [22].

The regions which appear light in Figs. 2 and 3 are due to ledeburite, formed by eutectic liquid solidification after the initial nucleation and

TABLE II Calculated volume fraction of primary austenite and ledeburite* in the RST powders

Alloy	Phase	Volume fraction for homogeneous case	Volume fraction for segregated case
2.4% C	Primary austenite	0.86	0.72
	Ledeburite	0.14	0.28
3.0% C	Primary austenite	0.59	0.49
	Ledeburite	0.41	0.51
3.0% C + 1.5% Cr	Primary austenite	0.42	0.41
	Ledeburite	0.58	0.59

*The calculations were based on knowing the carbon concentration of the eutectic liquid; these are 4.3% C for the 2.4% C and 3.0% C RST alloys and 4.1% C for the 3.0% C + 1.5% Cr RST alloy. In addition, for the homogeneous case, the equilibrium carbon concentration in austenite at the eutectic temperature was used; these are 2.1% C for the 2.4% C and the 3.0% C RST alloys and approximately 1.5% C for the 3.0% C + 1.5% Cr RST alloy. Also, for the segregated case, the carbon concentration in austenite at the eutectic temperature as determined from X-ray diffraction measurements on small powder particles was used; these are 1.67% C for the 2.4% C RST powder (also assumed to be the same for the 3.0% C RST powder) and 1.43% C for the 3.0% C + 1.5% Cr RST powder.

growth of cells and dendrites of primary austenite. Ledeburite is a mixture of carbide in a matrix of austenite. If the intercellular and interdendritic regions are thick enough (Figs. 2a and 3a), then the two-phase structure of carbide and austenite can be seen. In general, the intercellular and interdendritic regions are so thin and the carbides in the ledeburite so small that the two-phase structure is not generally apparent. The very fine size of the carbides in the ledeburite causes broadening of the carbide X-ray diffraction peaks. This broadening combined with the broadening of the austenite X-ray diffraction peaks (due to non-uniform distribution of carbon in the austenite) make the X-ray diffraction detection of the carbide in the ledeburite difficult. Thus, only faint carbide peaks were observed.

The acicular microstructure (Fig. 2e) is thought to be the result of the fastest cooling rates experienced by the smallest particles. This structure is thought to be a divorced eutectic structure in which the austenite solidifies from the eutectic liquid preferentially on primary cells and dendrites already formed and the carbides precipitate as needles. This divorced eutectic reaction takes place only in the particles with the smallest interdendritic spacing (i.e., the fastest cooled particles with the smallest amount of primary austenite).

4.2. Solute segregation

The volume fraction of constituents present, composed of primary austenite and ledeburite, is a function of the particle size (Figs. 2 and 3). More primary austenite is present in coarse particles than in fine powders. This is a direct consequence of the slower cooling rate of coarse particles compared to fine particles.

In the following, calculations were made to illustrate that the amount of austenite present can be estimated from the Fe–C [6, 24] and Fe–C–Cr [25] phase diagram by using the lever rule. Table II shows these calculations for the amounts of primary austenite and the ledeburite expected for each of the three powders. Calculations are given for two cases. The first case (under the column "homogeneous") is for large powder particles and the second case (under the column "segregated") is for small powder particles. In both cases, the calculations are made on the reasonable assumption that the solidified structure obtained at the eutectic temperature are retained at room temperature due to rapid cooling after complete solidification.

The calculations for the homogeneous case are based on the equilibrium carbon content at the eutectic temperature (2.1% C for the 2.4% C and 3.0% C powders and 1.5% C for the 3.0 C + 1.5% Cr powder). Such calculations can be expected to be applicable for large powder particles where the cooling rate is slow enough to allow sufficient time for carbon to diffuse and equilibrate in austenite during cooling from the liquidus to the eutectic temperature.

The calculations for the segregated case using the lever rule are based on the average carbon content of the retained austenite in small powder particles and are given in Table II. These calculations are based on the expectation that the small powder particles cooled so fast that the carbon in the primary austenite (in the austenite plus liquid

temperature region) did not have enough time to diffuse and reach the equilibrium value expected at the eutectic temperature. This leads to segregation, i.e., coring of carbon, in the primary austenite and has the effect of shifting the austenite solidus to lower carbon concentrations. This carbon segregation is responsible for the lesser amounts of primary austenite found in small particles.

The carbon content of the first austenite to solidify (i.e., at the liquidus temperature) is a function of the composition of the alloy and is 1.4% C for the 2.4% C powder, 1.5% C for the 3.0% C powder and 1.3% C for the 3.0% C + 1.5% Cr powder. The average carbon content of the retained austenite must lie between these values and the equilibrium carbon content of the austenite. This was found to be the case for the 2.4% C and 3.0% C + 1.5% Cr RST powders. Thus, the carbon content in austenite for small particles determined by X-ray diffraction measurements (1.67% C for the 2.4% C RST powder and 1.43% C for the 3.0% C + 1.5% Cr RST powder) does lie between the two extreme values mentioned.

The calculated values shown in Table II are in qualitative agreement with the observations made by SEM. Thus, more primary austenite is calculated for the homogeneous case (coarse powder particles) compared to the segregated case (fine particles) and this is in agreement with SEM observations (Fig. 2a and b). The results given in Table II also indicate that the amount of ledeburite in the 3.0% C RST alloy should be greater than that calculated for the 2.4% C RST white cast iron. This prediction is in qualitative agreement with SEM observations. Thus, photomicrographs for the 3.0% C RST powder, shown in Fig. 3, reveal a larger amount of ledeburite than is seen in photomicrographs for the 2.4% C RST powders (Fig. 2).

4.3. Effect of annealing on the microstructures

Annealing the RST powders at 650° C reveals that the primary austenite is metastable and quickly transforms to ferrite and carbide (Fig. 4). The carbides appear to occupy a much larger volume fraction of the matrix. This anomaly can be explained as an etching artifact [26] which leads to a higher than expected volume fraction of etch-resistant second phase.

The carbides have a bimodal carbide size distribution. The carbides that precipitate within the prior austenite cells and dendrites are smaller than the carbides that precipitate from the intercellular and interdendritic regions. The carbides that precipitate in the intercellular and interdendrite regions are coarser since these regions already contain carbide from the eutectic solidification whereas the primary cells and dendrites contain little or no carbide in the as-received condition.

Annealing time at 650° C changes the microhardness of the rapidly solidified powders as illustrated in Fig. 5. After a short time of annealing at 650° C, the microhardness decreases by a large amount corresponding to the large change in microstructure as seen by comparing, for example, Fig. 2 with Fig. 4a. Little change occurs in the microhardness and microstructure with further annealing. This indicates that the small carbides and alpha grains are relatively stable and grow slowly at 650° C. The high stability of fine grains in these RST powders allows the attainment of superplastic properties at intermediate temperatures [5]. The difference in the annealed microhardness (40 RC and 50 RC for 2.4% C and the 3.0% C + 1.5% Cr RST alloys, respectively) comes from two sources. The first and probably more significant one is the difference in the amount of carbide present. There is approximately 36 vol% carbide present in the annealed 2.4% C RST powders and 45 vol% carbide present in the 3.0% C RST powders. The second source is due to the solid solution strengthening contribution from the 1.5% Cr in the 3.0% C + 1.5% Cr RST alloy.

5. Conclusions

(1) The microstructure of rapidly solidified white cast irons consists principally of retained austenite and ledeburite.

(2) The average cooling rate of the powders was estimated to be about 3.3×10^5 °C sec^{-1}.

(3) The fast solidification rate in small powders causes carbon segregation in the austenite. When the eutectic temperature is reached, the austenite will have an average carbon concentration that is less than the value predicted for austenite at equilibrium at the eutectic temperature. This segregated primary austenite is retained with little further change as the temperature drops below the eutectic temperature and ultimately to room temperature.

(4) The intercellular and interdendritic regions consist of ledeburite, a mixture of retained austenite and carbides. The ledeburite and primary

austenite volume fractions in each RST alloy is in qualitative agreement with the values calculated from the measured average carbon content of the retained austenite.

(5) Only small quantities of martensite were observed in the rapidly solidified powders due to the low M_s temperature for high carbon austenite.

(6) The retained austenite in the RST powders transforms to a fine structure consisting of alpha iron and carbide at 650° C and the structure does not coarsen if annealed for several hours at the same temperature.

Acknowledgements

The authors gratefully acknowledge of this support of this programme by the US Office of Naval Research under Contract N00014-75-C-0662. They wish to thank especially Dr Bruce MacDonald of the ONR for his suggestions and guidance throughout all phases of this investigation. One of the authors (O.A.R.) would like to acknowledge support and co-operation from the Spanish Research Council (C.S.I.C.) and the Spanish–North American Joint Committee for Scientific and Technical Research. The white cast iron castings were provided by the Republic Steel Research Center, Independence, Ohio, USA, courtesy of Dr Don Byrd. The white cast iron powders were supplied by the Government Products Division of Pratt and Whitney, West Palm Beach, Florida, USA. The availability of the powders was made possible by the DARPA RSR Powders Program administered by Mr A. M. Adair of the AFML, Wright-Patterson Air Force Base, Ohio, USA.

References

1. National Materials Advisory Board, "Amorphous and Metastable Microcrystalline Rapidly Solidified Alloys: Status and Potential (NMAB 358)" (National Technical Information Service, Springfield, Virginia, 1980) pp. 1–10.
2. H. JONES, "Rapidly Quenched Metals", edited by N. J. Grant and B. C. Giessen (MIT Press, Cambridge, Massachusetts, 1976) p. 1–27.
3. R. MEHRABIAN, B. H. KEAR and M. COHEN (eds) "Rapid Solidification Processing Principles and Technologies II" (Claitors Publishing Division, Baton Rouge, Louisiana, 1980) pp. 1–23.
4. A. A. BOCHVAR, V. A. DAVIDOV and L. K. DRUZHININ, *Dokl. Acad. Nauk USSR* **230** (1976) 318.
5. O. A. RUANO, L. E. EISELSTEIN and O. D. SHERBY, *Met. Trans. A* **13A** (1982) 1785.
6. M. HANSEN, "Constitution of Binary Alloys" (McGraw-Hill, New York, 1958) p. 354.
7. J. WADSWORTH and O. D. SHERBY, *J. Mater. Sci.* **13** (1978) 264.
8. P. J. PATTERSON, A. R. COX and E. C. VAN REUTH, *J. Mat.* **32** (1980) 34.
9. "1979 Annual Book of ASTM Standards", Part 9, B213 (American Society for Testing and Materials, Pennsylvania, 1979).
10. B. D. CULLITY, "Elements of X-ray Diffaction" (Addison-Wesley, Reading, Massachusetts, 1967) p. 334.
11. "Metals Handbook", 9th Edn, Vol. 1 (American Society for Metals, Metals Park, Ohio, 1961) p. 77.
12. K. H. ZUM GAHR and W. G. SCHOLZ, *J. Met.* **32** (1980) 38.
13. D. J. DYSON and B. HOLMES, *J. Iron Steel Inst.* **208** (1971) 469.
14. M. C. RUHL and M. COHEN, *Trans. AIME* **245** (1969) 241.
15. P. H. SINGU, K. KOBAYASHI, K. SHIMOMURA and R. OZAKI, *Scripta Metall.* 8 (1974) 1317.
16. P. B. BOSWELL and G. A. CHADWICK, *J. Mater. Sci.* **11** (1976) 2287.
17. M. C. FLEMINGS, "Solidification Processing" (McGraw-Hill, New York, 1974) p. 49.
18. J. P. HIRTH, *Met. Trans. A* **9A** (1978) 401.
19. C. G. LEVI and R. MEHRABIAN, *ibid.* **13A** (1982) 221.
20. A. SUZUKI, T. SUZUKI, Y. NAGAOKA and Y. IWATA, *Nippon Kinzoku Gakkai-Si* **32** (1968) 1301.
21. C. Y. KUNG and J. J. RAYMENT, *Met. Trans. A* **13A** (1982) 328.
22. K. N. ANDREWS, *J. Iron Steel Inst.* **203** (1965) 721.
23. G. KRAUSS, "Principles of Heat Treatment of Steel" (American Society for Metals, Metals Park, Ohio, 1980).
24. "Metals Handbook", Vol. 8 (American Society for Metals, Metals Park, Ohio, 1973).
25. K. BUNGARDT, E. KUNZE and E. HORN, *Arch. Eisenhüttenw.* **29** (1958) 193.
26. C. KIM, V. BISS and W. F. HOSFORD, *Met. Trans. A.* **13A** (1982) 185.

Received 29 June
and accepted 12 July 1982